

RESEARCH

Open Access



# Stage-specific regulation of signalling pathways to differentiate pluripotent stem cells to cardiomyocytes with ventricular lineage

Ramakanth Satthenapalli<sup>1</sup>, Scott Lee<sup>1</sup>, Jayanthi Bellae Papannarao<sup>1</sup>, Timothy A. Hore<sup>2</sup>, Akash Chakraborty<sup>1,3</sup>, Peter P. Jones<sup>1</sup>, Regis R. Lamberts<sup>1</sup> and Rajesh Katare<sup>1\*</sup> 

## Abstract

**Background:** Pluripotent stem cells (PSCs) can be an ideal source of differentiation of cardiomyocytes in vitro and during transplantation to induce cardiac regeneration. However, differentiation of PSCs into a heterogeneous population is associated with an increased incidence of arrhythmia following transplantation. We aimed to design a protocol to drive PSCs to a ventricular lineage by regulating Wnt and retinoic acid (RA) signalling pathways.

**Methods:** Mouse embryonic stem cells were cultured either in monolayers or three-dimensional hanging drop method to form embryonic bodies (EBs) and exposed to different treatments acting on Wnt and retinoic acid signalling. Samples were collected at different time points to analyse cardiomyocyte-specific markers by RT-PCR, flow cytometry and immunofluorescence.

**Results:** Treatment of monolayer and EBs with Wnt and RA signalling pathways and ascorbic acid, as a cardiac programming enhancer, resulted in the formation of an immature non-contractile cardiac population that expressed many of the putative markers of cardiac differentiation. The population exhibited upregulation of ventricular specific markers while suppressing the expression of pro-atrial and pro-sinoatrial markers. Differentiation of EBs resulted in early foetal like non-contractile ventricular cardiomyocytes with an inherent propensity to contract when stimulated.

**Conclusion:** Our results provide the first evidence of in vitro differentiation that mimics the embryonic morphogenesis towards ventricular specific cardiomyocytes through regulation of Wnt and RA signalling pathways.

**Keywords:** Embryonic stem cells, Ventricular cardiomyocytes, Wnt signalling, Retinoic acid inhibition, Embryoid bodies

## Background

Cardiac regeneration via stem cell therapy is a promising field, and stem cell therapy using multipotent adult stem cells have been shown to ameliorate cardiac function. However, the efficacy of multipotent stem cells to differentiate into cardiovascular cells is still in debate, which is also reflected by the inconsistent results from

the clinical trials [1–3]. Pluripotent stem cells (PSCs) are a potential source of cardiovascular cells due to their ability to differentiate into functional cardiovascular cells in vitro, and hence in replacing the loss of cardiomyocytes as well as vascular cells due to ischemia [4, 5]. However, one of the major challenges, and one that has received very little attention, is the need to generate chamber-specific cardiomyocytes. This is critical, as different chambers in the heart have different functions. For instance, the right atrium contains the pacemaker cells and many conduction cells required to

\*Correspondence: [rajesh.katara@otago.ac.nz](mailto:rajesh.katara@otago.ac.nz)

<sup>1</sup> Department of Physiology, HeartOtago, School of Biomedical Sciences, University of Otago, 270, Great King Street, Dunedin 9010, New Zealand  
Full list of author information is available at the end of the article



© The Author(s) 2022. **Open Access** This article is licensed under a Creative Commons Attribution 4.0 International License, which permits use, sharing, adaptation, distribution and reproduction in any medium or format, as long as you give appropriate credit to the original author(s) and the source, provide a link to the Creative Commons licence, and indicate if changes were made. The images or other third party material in this article are included in the article's Creative Commons licence, unless indicated otherwise in a credit line to the material. If material is not included in the article's Creative Commons licence and your intended use is not permitted by statutory regulation or exceeds the permitted use, you will need to obtain permission directly from the copyright holder. To view a copy of this licence, visit <http://creativecommons.org/licenses/by/4.0/>. The Creative Commons Public Domain Dedication waiver (<http://creativecommons.org/publicdomain/zero/1.0/>) applies to the data made available in this article, unless otherwise stated in a credit line to the data.

initiate and conduct the electrical activity, respectively, whereas the ventricles are the heart's major pumping chambers containing the working cardiomyocytes. Unsurprisingly, our recent data show that the expression profiles of calcium handling proteins, crucial for contraction, are different between both chamber types in humans [6]. In general, PSCs yield a heterogeneous population of cardiomyocytes of which only 30–50% are ventricular cardiomyocytes [7, 8]. Since the majority of heart disease occurs in the ventricle, transplantation of a heterogeneous population with distinct functional and electrophysiological properties into the ventricle can contribute to cardiac arrhythmias [9, 10]. Recent animal studies have shown that exquisitely coordinated expression of various genes in a spatially and temporally controlled fashion is essential for normal cardiac development, with Wnt signalling, ascorbic acid (AA) and retinoic acid (RA) being key regulators of cardiogenesis [11, 12].

Wnt signalling has been reported to play a biphasic role in the differentiation of PSCs to cardiomyocytes where initial induction of Wnt signalling leads to the formation of mesoderm and the inhibition of Wnt signalling at later stages leads to differentiation to cardiomyocytes [13]. AA has been shown to enhance cardiac differentiation by upregulating the expression of transcription factors involved in the proliferation of cardiac progenitors in both mouse and human PSC models [14, 15]. On the other hand, RA has a significant role in specifying atrial and ventricular cardiomyocyte lineage in mouse and human PSCs. Positive signals of RA would lead to atrial specific cardiac differentiation, whereas inhibition of RA signalling drives the differentiation towards ventricular lineage [16]. These data therefore show that the individual modulation of Wnt, AA and RA signalling cascades can differentiate PSCs to cardiomyocytes. However, it is unknown whether combinatorial treatment with AA and temporal regulation of Wnt and RA signalling pathways, in a stage-specific manner, would lead to improved differentiation into a more homogeneous population of ventricular cardiomyocytes by suppressing the pacemaker population of cells. Therefore, the rationale of this study is to demonstrate if temporal regulation of Wnt and RA signalling pathway can differentiate PSCs to chamber-specific cardiac lineage.

In the current study, mouse embryonic stem cells (mESCs) were used as an in vitro PSC model. They were driven to cardiac lineage differentiation by regulating Wnt and RA signalling in the presence of AA as a cardiac programming enhancer. Cardiac differentiation in monolayer resulted in an immature non-contractile cardiac population that expressed all the putative markers of cardiac differentiation. They specifically exhibited

upregulation of ventricular specific markers while suppressing the expression of pro-atrial and pro-sinoatrial markers.

## Methods

### mESC culture and characterization

A transgenic TNG-A (a clone of transgenic Nanog) mESC strain and its corresponding predecessor control E14 mESC strain were used for all the experiments [17]. The TNG-A strain displays a green fluorescence protein (GFP) reporter tagged to one allele of the *Nanog* gene, whereby GFP expression corresponds to the expression of pluripotent protein Nanog (Additional file 1: Figure S1) [18]. The loss of GFP indicates the corresponding loss of pluripotent Nanog expression. The mESCs were seeded and expanded in culture dishes that were pre-coated with autoclaved and sterile-filtered 0.1% gelatin (Sigma-Aldrich, NZ). The mESCs were supplemented with mESC medium [High glucose Dulbecco's modified eagle's medium (DMEM, Thermofisher, NZ), 15% fetal bovine serum, 1X non-essential amino acids (Sigma-Aldrich, NZ), 100  $\mu$ M  $\beta$ -mercaptoethanol (Sigma-Aldrich, NZ), 1  $\mu$ g/ml puromycin, and 10 ng/ml leukemia inhibitory factor (LIF) (Thermofisher, NZ)]. The mESCs were maintained at 37°C in 5% CO<sub>2</sub> in a humidified normoxic environment. The cells were dissociated with TrypLE (Thermofisher, NZ) and passaged once every 3–4 days when they attained 70% confluency to avoid spontaneous differentiation induced by over confluency. mESCs were characterized for their pluripotency before exposing them to differentiation conditions (Additional file 1: Figure S2).

### Cardiac differentiation of mESCs

#### Monolayer differentiation

mESCs (200,000 cells/well) were seeded in a 24-well plate and allowed to grow for 3 days until they reached 80% confluent. To induce cardiac differentiation, the culture medium was replaced with serum-free medium, and cells were treated with AA (Sigma-Aldrich, NZ), IWP2 (Wnt inhibitor (Wi), Sigma-Aldrich, NZ) and BMS-189453 (RA inhibitor (RAi), Sigma-Aldrich, NZ) at different points as shown in Fig. 1A. Cells were harvested on days 3, 5, 9 and 14 for characterization.

#### Three-dimensional (3D) differentiation by embryoid body (EB) formation

EBs were generated using the three-dimensional hanging drop (HD) technique. For this, mESCs (1000 cells/10  $\mu$ L) were suspended in the EB differentiation medium and placed as a drop (10  $\mu$ L) on the inner side of the lid of a petri dish (Sigma-Aldrich, NZ). Around 40–50 drops were evenly placed per dish (Fig. 1B). The base of the

petri dish was filled with 10 mL of sterile 1X phosphate buffered saline (PBS) as a source of humidity to the cell cluster in the hanging drops. The lid was then inverted, closed and cultured at 37 °C in a 5% CO<sub>2</sub> incubator. Spherical EBs were visibly formed by day 2. The EBs on day 3 were gently flushed and plated on uncoated Petri dishes in EB differentiation medium supplemented with AA and Wi followed by treatment with RAi as shown in Fig. 1B.

#### Quantitative real time-PCR (RT-PCR) analysis

Total RNA isolated using TRIzol (ThermoFisher) was reverse-transcribed using PrimeScript™ RT Reagent Kit (Takara Bio, Japan). The resulting cDNA was amplified using SYBR green premix Ex Taq II (Takara Bio, Japan) in StepOne plus PCR machine (Thermo Fisher Scientific, USA) to quantify the expression of genes associated with pluripotency (*Nanog*, *Oct4* and *Sox2*) and cardiac differentiation (Kinase Insert Domain Receptor (*KDR*), mesoderm posterior protein 1 (*Mesp-1*), islet-1 (*Isl-1*), *Nkx2.5*, *T-Box Transcription Factor 5* (*Tbx5*), cardiac Troponin-T (*cTnT*), Myosin Regulatory Light Chain 2 Atrial isoform (*MLC-2a*), Myosin regulatory Light Chain 2 Ventricular isoform (*MLC-2V*), and Iroquois Homeobox 4 (*IRX4*). The day 0-mESCs was used as a negative control for the experiment to normalize the transcript levels of differentiated cells. The entire differentiation process, sample processing, and qPCR were independently repeated three times ( $n = 3$ ). Data are presented as log fold change to day 0-mESCs. The list and sequence of all the primers used in this study are listed in Additional file 1: Table S1.

#### Flow cytometry analysis

Cells in suspension were fixed with 4% PFA for 20 min at room temperature and probed with antibodies against pluripotency markers (Oct3/4, Sox2) and cardiac differentiation markers (T brachyury (T-Bry), KDR, ISL-1, Nkx2.5, cTnT, IRX4, MLC2V and connexin-43 (Cx43)). Details of antibodies, including the concentration used, are listed in Additional file 1: Table S2. To compensate for the use of multiple fluorescent antibodies, single stain

controls comprising of antibody capture beads were used (AbC™ anti-mouse bead kit, Thermo Fischer Scientific, USA). Cell acquisition was performed using the flow cytometer (Gallios, Beckman Coulter Inc., USA). In total, 5000 to 50,000 events within the gate of interest were acquired depending on the sample type. Flow cytometer voltages were set using an unstained, single stained bead or secondary antibody controls so that the spill-over was minimum in the adjacent channels. Post-acquisition compensation and data analysis were performed using Flowjo 10.6.1 software (TreeStar, USA) [19].

#### Immunofluorescence analysis

Monolayer cells seeded on glass coverslips in a 24-well plate were fixed with 4% PFA and permeabilized with pre-chilled methanol for intracellular staining. The cardiac cells of EBs were dissociated by collagenase IV/Trypsin treatment, singularized and seeded onto 0.1% gelatin-coated coverslips before fixation and permeabilization. After blocking with either 10% serum or 1%BSA, cells were incubated with primary antibodies against Nkx2.5, Cx43,  $\alpha$ -sarcomeric actin, IRX4 and MLC2V (all antibodies and concentrations listed in Additional file 1: Table S2) and incubated overnight at 4 °C. After washing, the cells were probed with secondary antibodies (1:500 dilution) conjugated with Alexa flour. Finally, cells were stained with DAPI (0.1 ug/mL, Thermo Fischer Scientific, USA) to visualize the nuclei and mounted on glass slides using Fluoromount G (Southern Biotech, USA). Images were captured in NikonA1R Resonant Scanner confocal microscope and analysed using ImageJ software, version 1.52 (NIH, USA). A control group for secondary antibodies (with the same labelling procedure without the primary antibody treatment, Additional file 1: Figure S3) was used to rule out the non-specific binding of the secondary antibody.

#### Transmission electron microscopy (TEM)

The cells were fixed in 2.5% glutaraldehyde (primary fixative) and 1% osmium tetroxide (secondary fixative) dissolved in sodium cacodylate buffer. Post-fixation,

(See figure on next page.)

**Fig. 1** Schematic diagram of the protocols to differentiate mESCs to cardiovascular lineage. **A** Monolayer differentiation of mESCs to cardiomyocyte lineage. The mESCs were cultured in mESC growth medium (MGM) for three days (day – 3 to 0). On day 0, the medium was replaced with RPMI/ B27-insulin as the serum-free differentiation medium (SFDM). Cells were treated with ascorbic acid (AA) from day 0, which continued until the end of the differentiation protocol (day 14). From days 3–5, cells were treated Wnt inhibitor (Wi), and from days 6–9, they were treated with retinoic acid inhibitor (RAi). **B** Three-dimensional differentiation of mESCs by EB method. EBs were generated by the hanging drop technique. On day 0, mESCs were dissociated, counted, and pipetted as drops of media on the inner side of a petri dish lid. The lid was inverted, and the petri dish was closed to form hanging drops. On day 2, spherical EBs was formed. On day 3, EBs were flushed with SFDM and cultured in suspension in an uncoated petri dish. On day 5, EBs were transferred to a 24-well plate containing 0.1% gelatin-coated coverslips. From day 5 to 30, EBs were cultured and differentiated in a monolayer. From day 6–9, cells were treated with RAi.

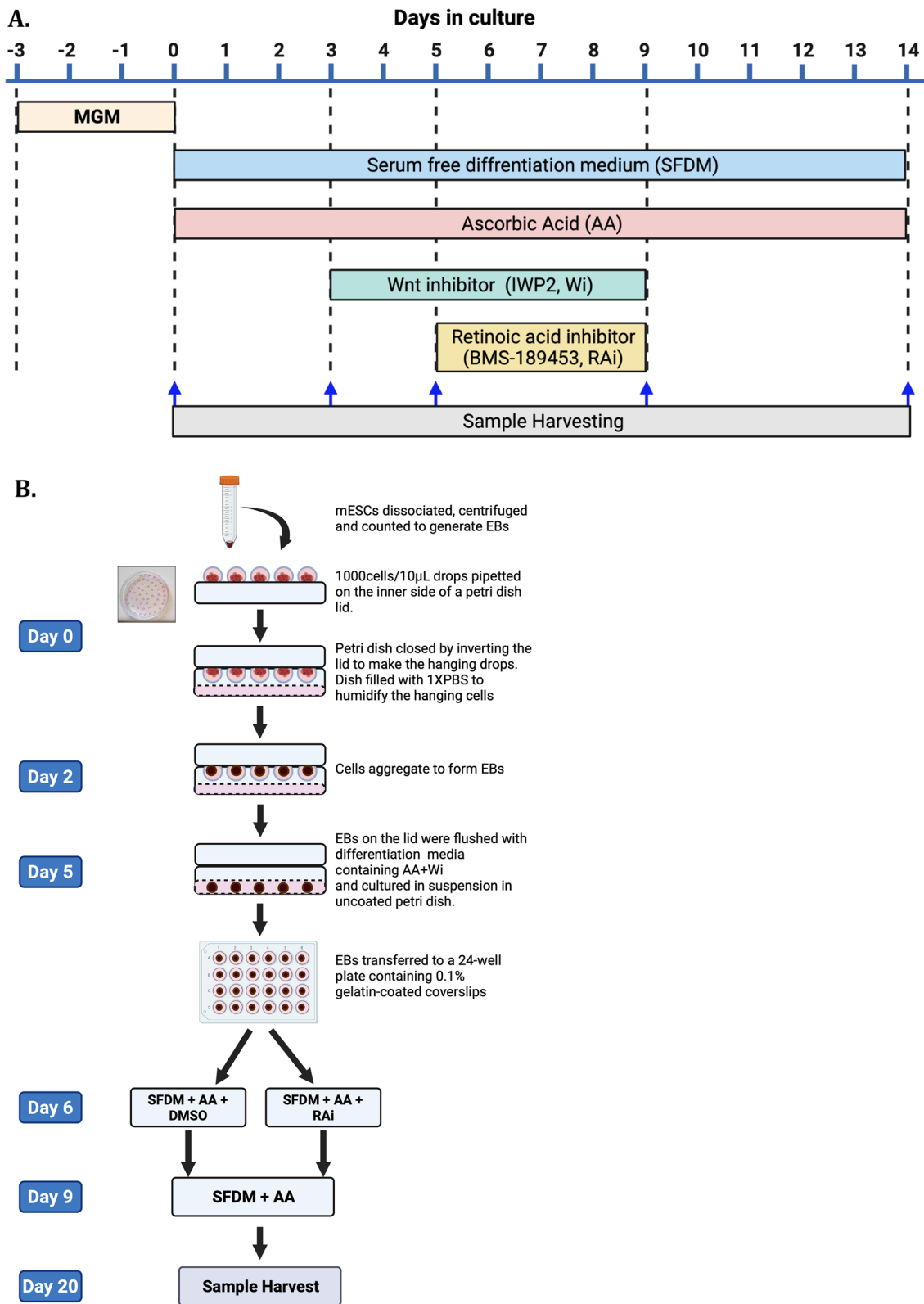


**Fig. 1** (See legend on previous page.)

the cells were dehydrated by washing with an ethanol series (50/70/90/100% ethanol, 5 min each). The cells were then treated with 100% propylene oxide, resin infiltrated, embedded in resin-filled silicone moulds, and finally were cured at 60 °C for 48 h. Post-curing, ultrathin sections (85 nm) were cut with an ultramicrotome (Leica EM UC7) and transferred to a copper grid (Sigma-Aldrich, NZ). The sections were then stained with 4% uranyl acetate for 25 min, rinsed in Milli-Q water, and transferred to 1% lead citrate for 5 min before rinsing in Milli-Q water and air drying. Images were captured with a Philip CM100 BioTWIN transmission electron microscope (Philips/FEI Corp., Eindhoven, Holland). The following parameters were measured; cell area ( $\mu\text{m}^2$ ), perimeter ( $\mu\text{m}$ ), and circularity index [20]. The differentiated cells were identified based on the presence of multinucleated cardiac cells, increased cell size (area and perimeter), reduced circularity index, increased mitochondrial number, the presence of lipid droplets and glycogen bodies as some of the putative morphological characteristics observed during cardiac differentiation.

#### Cytosolic $\text{Ca}^{2+}$ imaging of differentiated cardiac cells

To measure the cytosolic  $\text{Ca}^{2+}$ , differentiated cells were loaded with fluo-4-AM (2  $\mu\text{M}$ , Thermofisher, NZ), a cell-permeable acetoxymethyl ester (AM) form of  $\text{Ca}^{2+}$  indicator for 10 min at room temperature. Cells were then washed twice with Krebs–Ringer HEPES (KRH) buffer to remove any de-esterified dye. Fluorescence of fluo-4 was detected by imaging the cells using CoolSNAP HQ2 CCD camera (Nikon). The analysis of cytosolic  $\text{Ca}^{2+}$  imaging was done using NIS-Elements AR Analysis 4.00.03 64-bit software (Coherent Scientific Pty. Ltd, Australia).

#### Western blot analysis

mESCs at different time points of differentiation were homogenized in ice-cold RIPA lysis buffer supplemented with a 1% protease inhibitor cocktail (Sigma Aldrich, USA) [21]. The total protein was quantified by Bradford protein assay (BioRad, New Zealand). Twenty micrograms of protein were resolved by 15% SDS-PAGE and transferred to polyvinylidene fluoride

membrane. After blocking and confirming the successful transfer of proteins using ponceau staining, membranes were probed with primary antibodies against CX43 (1:1000 dilution, Sigma Aldrich), MLC2V (1:1000 dilution, Abcam), and  $\beta$ -actin (1:1000 dilution, Santa Cruz Biotechnologies) overnight at 4 °C. Goat anti-rabbit secondary antibody (1:10,000 dilution, Abcam) was used for detection. The density of bands was analysed using ImageJ (NIH, United States) software and normalized to GAPDH.

#### Experimental repeats and statistical analysis

The experimental repeats ( $n$ ) were assay dependent. Quantitative real-time PCR, flow cytometry, and calcium imaging assays were performed with three independent repeats ( $n=3$ ). For TEM analysis, 10 cells in each sample were used for analysis. Spontaneous  $\text{Ca}^{2+}$  activity in the stimulated EBs was performed with at least 8 EBs. All the statistical analyses were done using Graph Pad Prism 9 software. Statistical significance was determined by (1) Student's  $t$ -test to identify the difference between two groups (2) a one-way ANOVA with Dunnett's or Sidak's multiple comparison post hoc test to identify the difference when there were more than two groups, and (3) a two-way ANOVA with Tukey's or Sidak's multiple comparison post hoc test to compare more than two groups with two independent variables. Data are presented as mean  $\pm$  SEM.  $P < 0.05$  was considered statistically significant.

## Results

### Monolayer differentiation of mESCs

#### Stage-specific expression of differentiated markers

Serial monitoring of mESCs demonstrated the upregulation of putative cardiovascular markers in a stage-specific manner. qPCR analysis showed significant downregulation of the expression of pluripotent gene *Oct4* (Fig. 2A) and *Nanog* (Additional file 1: Figure S3) from day 9 of differentiation. AA treatment from day 0–3 (Fig. 1A) induced upregulation of cardiovascular precursor gene *KDR* (Fig. 2B). Wnt inhibition from day 3 (Fig. 1A) induced upregulation of cardiac mesoderm specific gene *Mesp-1* from day 5 (Fig. 2C). Further, Wnt inhibition induced upregulation of cardiac progenitor genes *Isl-1* (Fig. 2D) and *Nkx2.5* (Fig. 2E) and ventricular progenitor gene *Tbx5* (Fig. 2F), suggesting differentiation towards cardiac phenotype and, in particular, ventricular phenotype. The expression of both *Isl-1*

(See figure on next page.)

**Fig. 2** RT-PCR analysis of cardiac differentiation markers. Quantitative scatter plot bar graphs showing the expression of stage-specific cardiac differentiation genes on day 0, 3, 5, 9 and 14 following differentiation of mESCs in monolayers. The data were normalized to the gene expression of mESCs on day 0. Data were analysed by one-way ANOVA, Dunnett's multiple comparisons test, \* $P \leq 0.05$ , \*\* $P < 0.01$ , \*\*\* $P < 0.001$  and \*\*\*\* $P < 0.0001$  versus day 0 samples;  $\delta < P < 0.05$ ,  $\delta\delta P < 0.001$  versus day 3 samples; # $P < 0.05$  versus day 9 samples.  $n = 4$  independent repeats

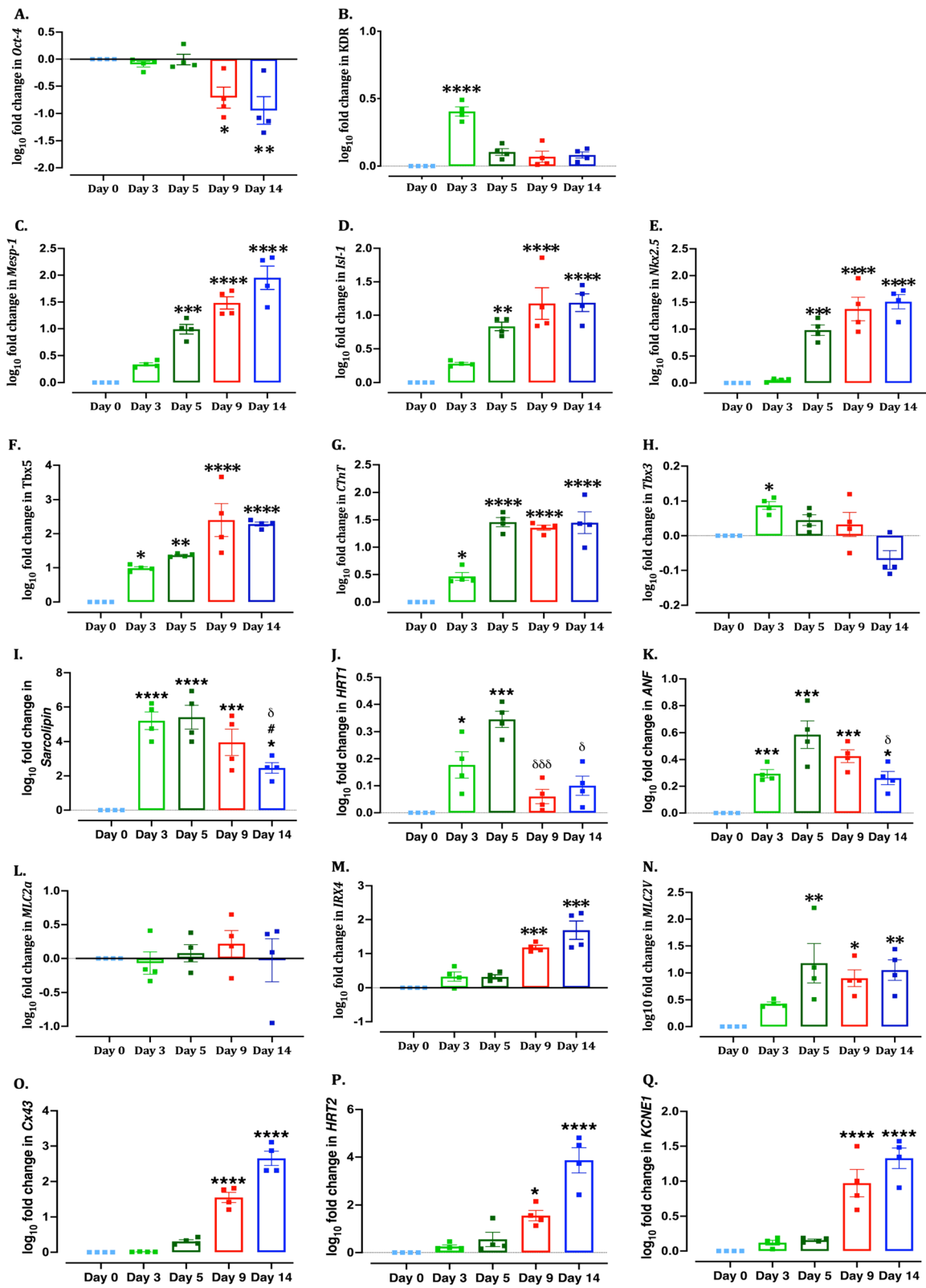


**Fig. 2** (See legend on previous page.)

and *Nkx2.5* remained upregulated until 14 days of differentiation (Fig. 2D&E), suggesting the cells still retain their progenitor phenotype. With the progression of differentiation, there was a significant upregulation of cardiac structural gene *cTnT* (Fig. 2G) as early as day 3, highlighting the importance of AA in initiating cardiac differentiation by increasing the number of CPC (also reported by Cao et al. [15]). While AA treatment-induced initial upregulation of pro-sinoatrial gene *Tbx3* (Fig. 2H) and atrial specific genes *Sarcolipin* (Fig. 2I), *HRT1* (Fig. 2J) and *ANF* (Fig. 2K), these were significantly downregulated following treatment with Wnt and RA inhibitors (Fig. 2H–K). Another atrial specific gene *MLC2a* showed no difference at any stage of differentiation (Fig. 2L). The ventricular specific differentiation of mESCs was further confirmed by significant upregulation of ventricular specific genes *IRX4* (Fig. 2M), *MLC2V* (Fig. 2N), *Cx43* (Fig. 2O), *HRT2* (Fig. 2P) and *KCNE1* (Fig. 2Q). The upregulation of *IRX4*, *Cx43*, *HRT2* and *KCNE1* following treatment with RAi (Fig. 1A) highlights the inverse correlation between RA signalling and differentiation towards ventricular lineage and may indicate why the presence/absence of RA signalling would affect the atrial/ventricular cardiac population.

Importantly, observed changes in the gene expression was translated to proteins showing significant upregulation of cardiac transcription factors (*Isl-1* (Fig. 3A, B) and *Nkx2.5* (Fig. 3A)), structural protein (*CTnT* (Fig. 3B)), contractile protein ( $\alpha$ -sarcomeric actin ( $\alpha$ -SA, Fig. 3A)) and ventricular specific proteins (connexin-43 (Fig. 3A, C and Additional file 1: Figure S8), *Tbx5* (Fig. 3A), *IRX4* (Fig. 3B), *Mef2c* (Fig. 3B) and *MLC2V* (Fig. 3D and Additional file 1: Figure S8) as observed by immunofluorescence at different time points (Fig. 3A) and on day 14 by flow cytometry (Fig. 3B) and western blot (Fig. 3C, D) analysis.

We further confirmed that mESCs do not "spontaneously" differentiate into cardiac lineage when cultured for 14 days in the absence of signalling regulators (Additional file 1: Figure S4).

#### **The ultrastructure of differentiated mESCs revealed early-stage cardiomyocytes features**

Differentiated mESCs (Fig. 4E–H) were larger compared to the small spherical undifferentiated mESCs

(Fig. 4A–D) and displayed heterogeneous shapes (spherical, triangular or cylindrical) (Fig. 4E–H). Quantitative analysis showed an increase in cell area ( $83.18 \pm 5.107 \mu\text{m}^2$  vs  $600 \pm 53.32 \mu\text{m}^2$ ,  $P < 0.0001$ ) and perimeter ( $30.7 \pm 1.075 \mu\text{m}$  vs  $119.4 \pm 6.596 \mu\text{m}$ ,  $P < 0.0001$ ), as well as decrease in circularity index ( $0.916 \pm 0.004$  vs  $0.547 \pm 0.05$ ,  $P < 0.0001$ ) (Fig. 4I–L). The majority of the differentiated cells were multinucleated, which is crucial before neonatal CMs are terminally differentiated. In contrast to the spherical immature mitochondria with little or no cristae in the undifferentiated mESCs (Fig. 4D), the mitochondria in the differentiated cells showed crisp membrane structures and cristae formation (Fig. 4H) and were high in number (Fig. 4L). The large number, size and mature cristae in the mitochondria of the differentiated cells could be attributed to their high demand for oxidative phosphorylation and hence, ATP production.

#### **Cardiac differentiation of mESCs from EBs**

Monolayer differentiation did not show any maturation in morphology (Fig. 4) or  $\text{Ca}^{2+}$  activity (Additional file 1: Figure S5), which may be attributed to the monolayer cell culture not representing the in vivo embryonic niche. We next induced cardiac differentiation of mESCs using the EB method, which provides a 3D environmental niche. EB-differentiated mESCs exhibited mature morphology compared to the cells differentiated in monolayers (Additional file 1: Figure S6). This was also confirmed by immunofluorescence analysis of cardiac transcription factors *Nkx2.5* (Additional file 1: Figure S7A) and *Isl-1* (Additional file 1: Figure S7B), and ventricular lineage markers *IRX4* (Additional file 1: Figure S7C), *MLC2V* (Additional file 1: Figure S7C), *Mef2c* (Additional file 1: Figure S7D) and *Cx43* (Additional file 1: Figure S7E). Flow cytometry analysis also confirmed the expression of *IRX4* (Additional file 1: Figure S7F) and structural protein *cTnT* (Additional file 1: Figure S7F). Using this model, we determined the importance of RA inhibition (RAi) in ventricular specific differentiation of mESCs.

(See figure on next page.)

**Fig. 3** Expression of cardiomyocyte proteins. **A, B** Representative immunofluorescence and flow cytometry images showing the expression of cardiac transcription factors (*Isl-1*, *Nkx2.5*), cardiac structural protein (cardiac troponin T, *cTnT*), cardiac contractile protein ( $\alpha$ -sarcomeric actin,  $\alpha$ -SA) and left ventricular specific proteins (connexin-43, *Tbx5* and *IRX4*) at on days 3, 5, 9 and 14 of differentiation. Secondary control was used as an experimental negative control in the absence of primary antibody to negate the non-specific binding of the secondary antibody and rule out false positive expression (Additional file 1: Figure S3). Nuclei were stained with DAPI. Initial green colour is due to the endogenous expression of GFP tagged pluripotent Nanog protein which gradually reduces and disappears with differentiation of cells. Positive staining is indicated by red colour. Scale bar = 50  $\mu\text{m}$ . **C, D** Representative western blot images and quantitative scatter plot bar graphs showing the expression of ventricular specific proteins *Cx43* (**C**) and *MLC2V* (**D**) at different time points

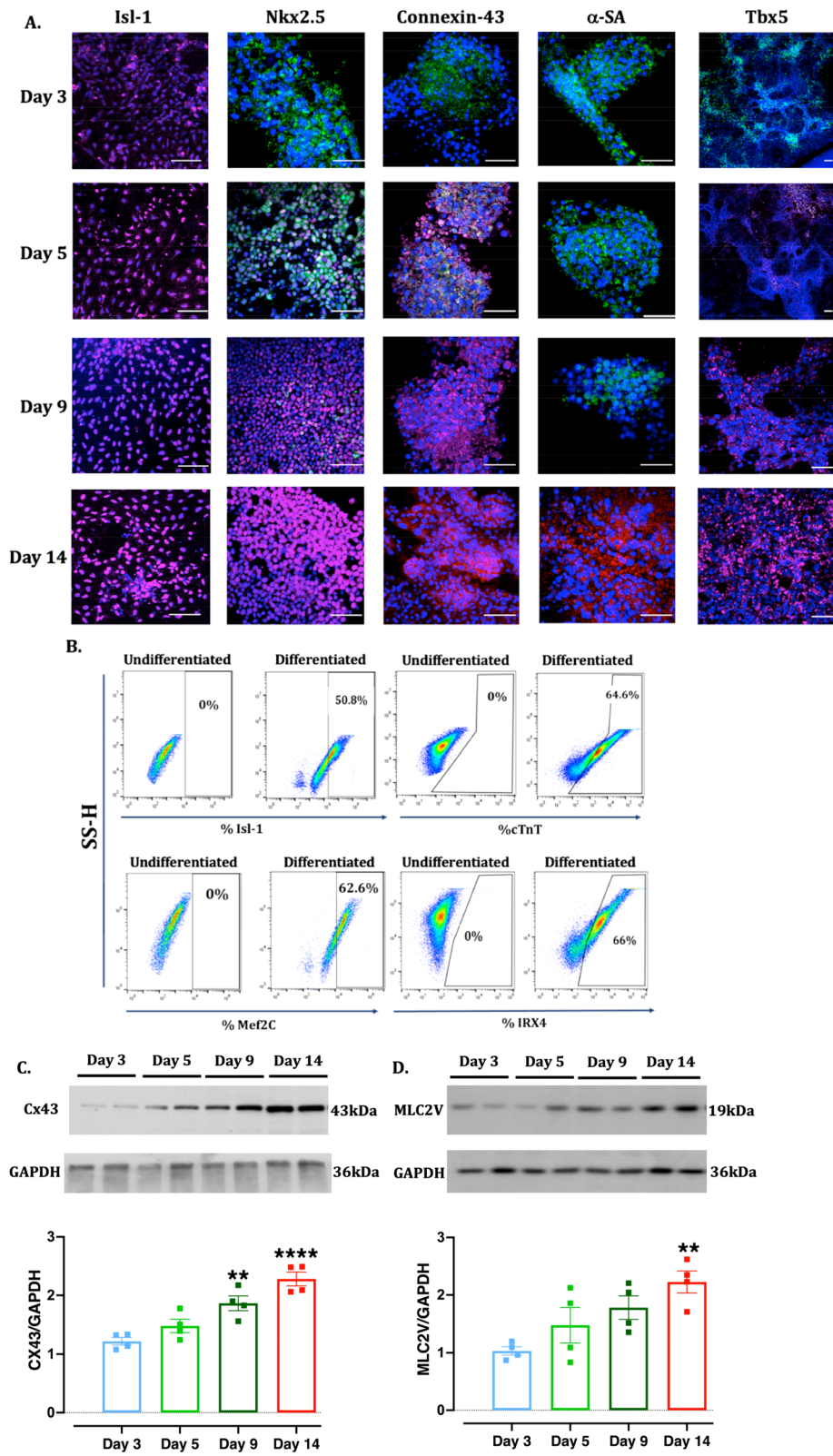


**Fig. 3** (See legend on previous page.)



### EB-differentiated mESCs displayed spontaneous contractility and cytosolic Ca<sup>2+</sup> activity

In contrast to the cells differentiated in monolayers, EB-differentiated mESCs which were not treated with RA inhibitor (-RAi) showed spontaneous contractility, while this was not observed in the EB treated with RA inhibitor (+RAi, Fig. 5A). The area under the curve of averaged contracting EBs increased to  $565 \pm 25.2$  in +RAi cells after 20 days of differentiation compared to  $26.7 \pm 5.8$  -RAi cells ( $P < 0.001$ ). This correlated with the spontaneous Ca<sup>2+</sup> peaks in the -RAi (Fig. 5B) and higher expression of calcium release channel ryanodine receptor 2 (*RyR2*) (Fig. 5D). Spontaneous Ca<sup>2+</sup> peaks were not observed in +RAi cells (Fig. 5B). However, when electrically stimulated, both -RAi and +RAi EBs demonstrated spontaneous contraction and hence the spontaneous Ca<sup>2+</sup> peaks (Fig. 5C).

### RAi downregulated sinoatrial and atrial specific gene/protein expression

Similar to the monolayer differentiation, RT-PCR analysis confirmed the downregulation of pluripotent gene *Oct4* (Fig. 6A) and upregulation of cardiac progenitor gene *Nkx2.5* (Fig. 6B) and structural gene *cTnT* (Fig. 6C) in both +RAi and -RAi groups. The +RAi group showed a significant upregulation in the expression of ventricular-specific progenitor gene *Tbx5* (Fig. 6D). At the same time, there was no significant difference in the expression of adult ventricular genes *IRX4* (Fig. 6E) and *MLC2V* (Fig. 6F) between the groups. However, RA inhibition prevented the upregulation of pro-atrial (*Isl-1* (Fig. 6G) and *MLC2a* (Fig. 6H)) and sinoatrial genes (T-box transcription factor 3 (*Tbx3*)) (Fig. 6I). This is supported by the absence of contracting EBs in +RAi EBs (Fig. 5A). These results suggest that AA and Wnt inhibition is sufficient to drive the differentiation towards ventricular phenotype. However, RA inhibition could act as a determining step to downregulate atrial and nodal subtypes in the differentiated cells, thus driving the cells towards ventricular specific differentiation.

### RA inhibition increased mature cardiomyocytes phenotype of differentiated mESCs

Like monolayer-differentiated mESCs, the EB-differentiated mESCs were multinucleated with increased mitochondrial number and length, accumulation of lipid droplet, glycogen granule deposition, the SR calcium stores, and presence of clusters of rough-ER (Fig. 7A–J).

Compared to -RAi cells, +RAi cells displayed a larger cell area (mean =  $343 \pm 28 \mu\text{m}^2$  vs mean =  $929 \pm 57 \mu\text{m}^2$ ,  $P < 0.0001$ , Fig. 7K) and perimeter (mean =  $80 \pm 5 \mu\text{m}$  vs mean =  $180 \pm 10 \mu\text{m}$ ,  $P < 0.0001$ , Fig. 7L), and significantly smaller circularity index (mean =  $0.6 \pm 0.04$  vs  $0.41 \pm 0.05$ ,  $P = 0.006$ , Fig. 7M) suggesting a morphologically mature cardiomyocyte phenotype with RA inhibition. The mitochondrial number was not significantly different between both groups (Fig. 7N). Further, both the groups showed the presence of collagen fibrils following differentiation (Fig. 7E and J).

### Discussion

We have developed a unique combinatorial protocol to differentiate mESCs to cardiovascular lineage in a stage-specific manner. Although there are a plethora of protocols to differentiate PSCs to heterogeneous cardiomyocyte populations (nodal, atrial, and ventricular), to our knowledge, this is the first study to develop a protocol to differentiate PSCs to cardiomyocytes that are oriented towards ventricular-lineage without automaticity, via sequential modulation of the Wnt and RA signalling pathway in the presence of AA [15, 22, 23]. In this study, we differentiated the cells by growing them in monolayers and in EBs. In both models, RAi played a crucial role in differentiating the mESCs to a ventricular specific phenotype.

Using the monolayer cardiac differentiation protocol, we were able to demonstrate a stage-specific upregulation of cardiovascular precursors (*KDR* and *Mesp-1*), cardiac progenitors (*Isl-1*, *Nkx2.5*, and *Tbx5*), and ventricular cardiomyocyte markers (*Tbx5*, *IRX4*, and *MLC2V*) and downregulation of pluripotent markers (*Oct-4* and *Nanog*). Our results showed that AA specifies cardiovascular fate in mESCs, and inhibition of Wnt signalling induces cardiac mesoderm population. This is likely due to the interplay of epigenetic changes in DNA methylation of cardiac genes such as *Isl-1* and the integrin signalling system [24]. In support of this, *Isl-1* expression was upregulated at both gene and protein level as early as day 3 of differentiation in our study. Myocyte enhancer factor 2C (*Mef2C*) is a direct transcriptional target of *Isl-1*, and the expression of *Mef2C* is a sign of gradual cardiac looping morphogenesis during in vitro cardiac differentiation [25]. Sustained increase in *Mef2C* protein expression from day 3 to 14 of differentiation in our study signifies that the cardiac cells were undergoing an event of morphogenesis throughout the

(See figure on next page.)

**Fig. 4** Ultrastructural features of mESCs differentiated in monolayers. **A–H**—representative transmission electron microscopy pictures of undifferentiated (**A–D**) and differentiated (**E–H**) mESCs. N—nucleus; M—mitochondria; ER—endoplasmic reticulum. **I–L**—quantitative scatter plot bar graphs showing cell area (**I**), perimeter (**J**), circularity index (**K**), and mitochondrial number (**L**). Data were analysed by unpaired t-test with Welch's correction. Data presented as mean  $\pm$  SEM. \*\*\*\* $P < 0.0001$  versus undifferentiated cells.  $n = 10$  cells in each group

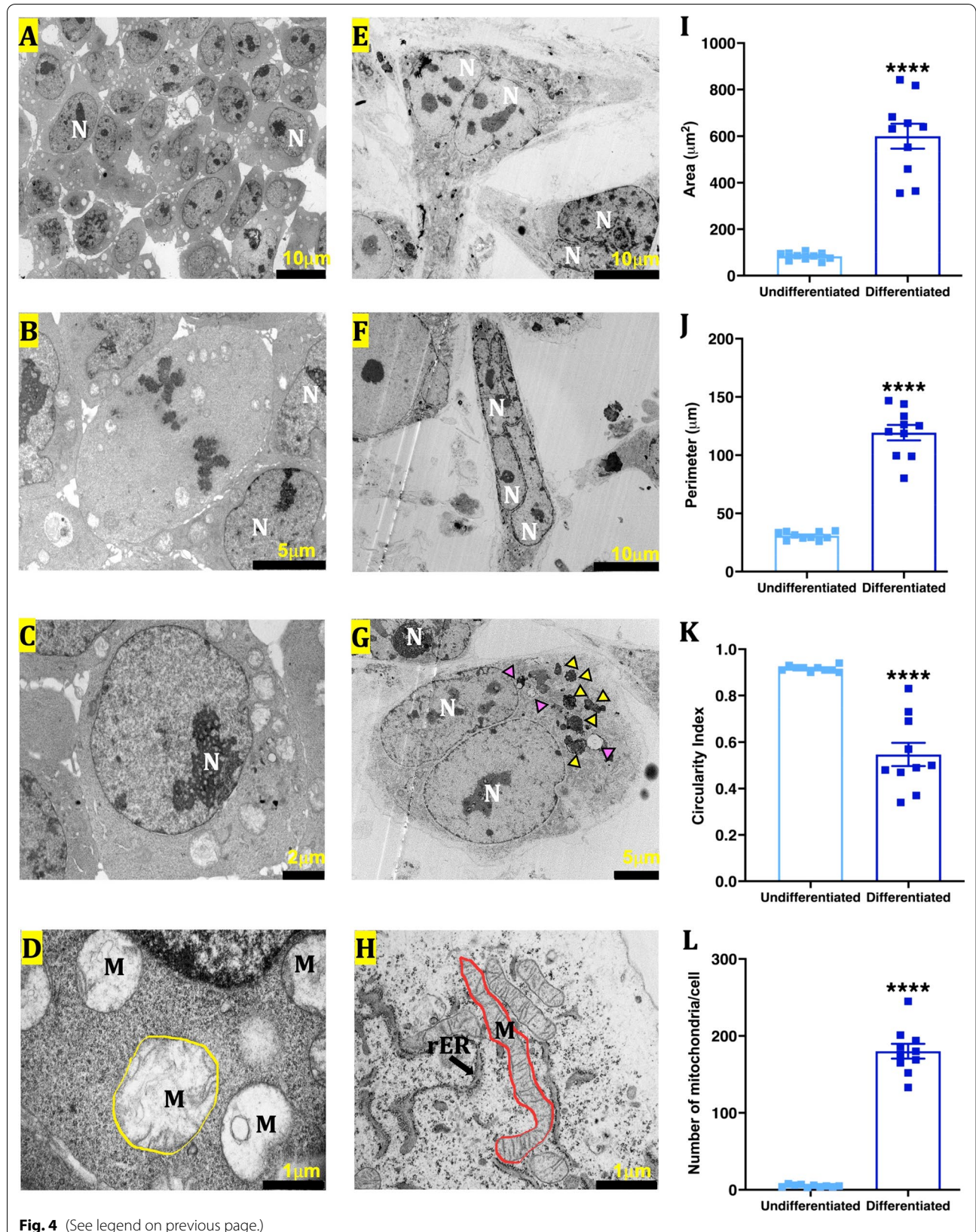


**Fig. 4** (See legend on previous page.)

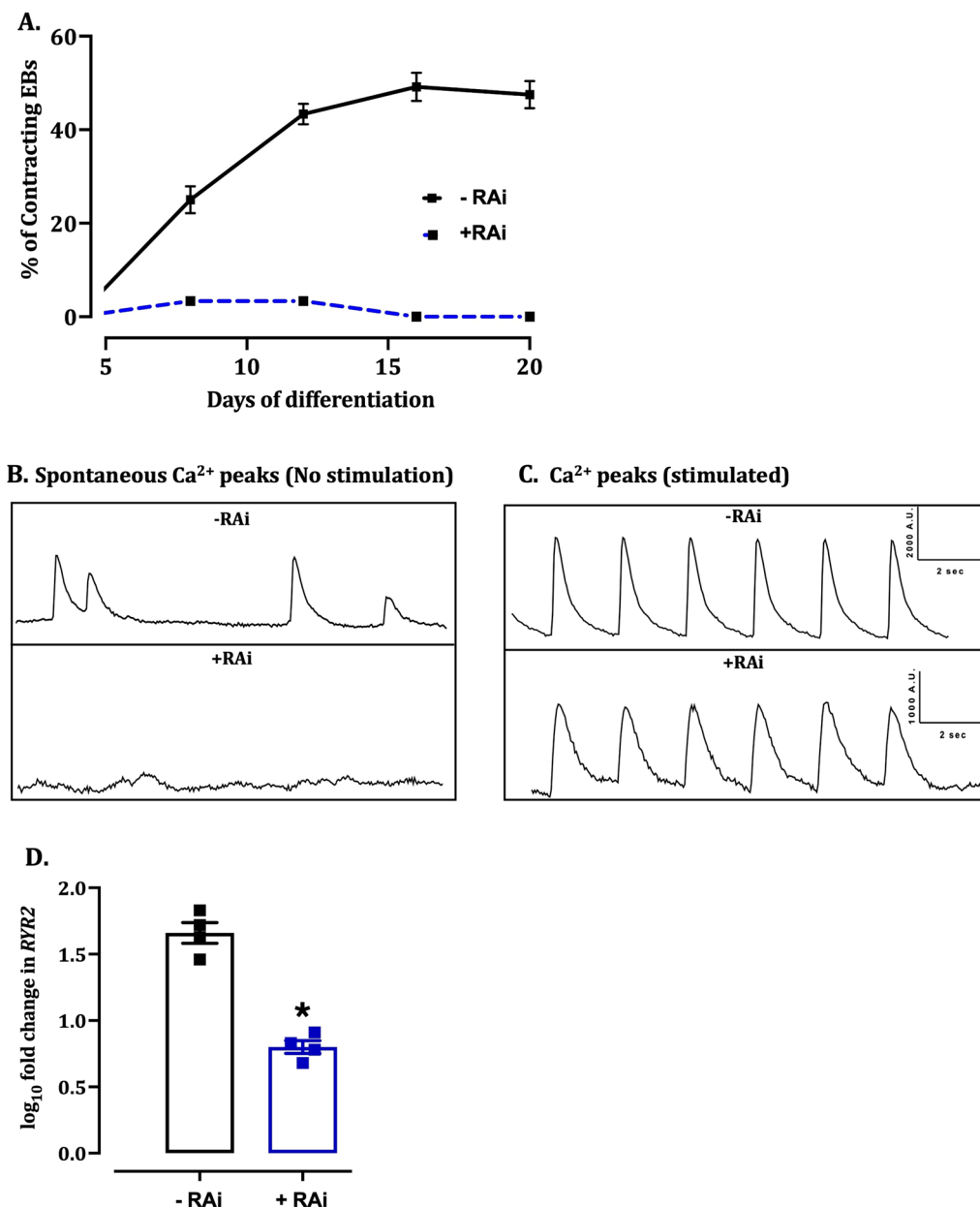


**Fig. 5** Characterization of mESCs differentiated by EB. **A** Quantitative line graphs showing the percentage of contracting EBs treated with RA inhibitor (+RAi) or control (−RAi). Data were analysed by two-way ANOVA and presented as Mean ± SEM. \**P* < 0.05 versus previous time point; #*P* < 0.05 versus +RAi group at corresponding days. **B, C** Representative Ca<sup>2+</sup> traces of a single EB dissected from −RAi and +RAi groups. The EBs were treated with Fluo-4 and electrically stimulated to visualize spontaneous Ca<sup>2+</sup> release as functional characterization of contracting CMs. **D** Quantitative scatter plot bar graphs of RT-PCR analysis showing the expression of RYR2 in the treatment groups. Data were analysed by unpaired *t*-test with Welch’s correction and presented as mean ± SEM. \**P* < 0.05 versus −RAi group. *n* = 4 independent repeats

differentiation. *Nkx2-5* is one of the earliest known transcription factors required for cardiac cell specification and maintains the ventricle chamber identity. *Nkx2.5* mutants had a reduced number of ventricular cardiomyocytes and excess atrial cells [26]. The double mutants for *Nkx2-5* and Heart and Neural Crest Derivatives Expressed 2

(*HAND2*) were shown to completely abolish the expression of the ventricular-specific homeobox gene *Irx4*. *Nkx2.5* is also reported to be essential in maintaining the ventricle chamber identity [26, 27]. This evidence reiterates the significance of *Nkx2.5* expression in early cardiac mesoderm specification, proliferation, heart tube morphogenesis, and

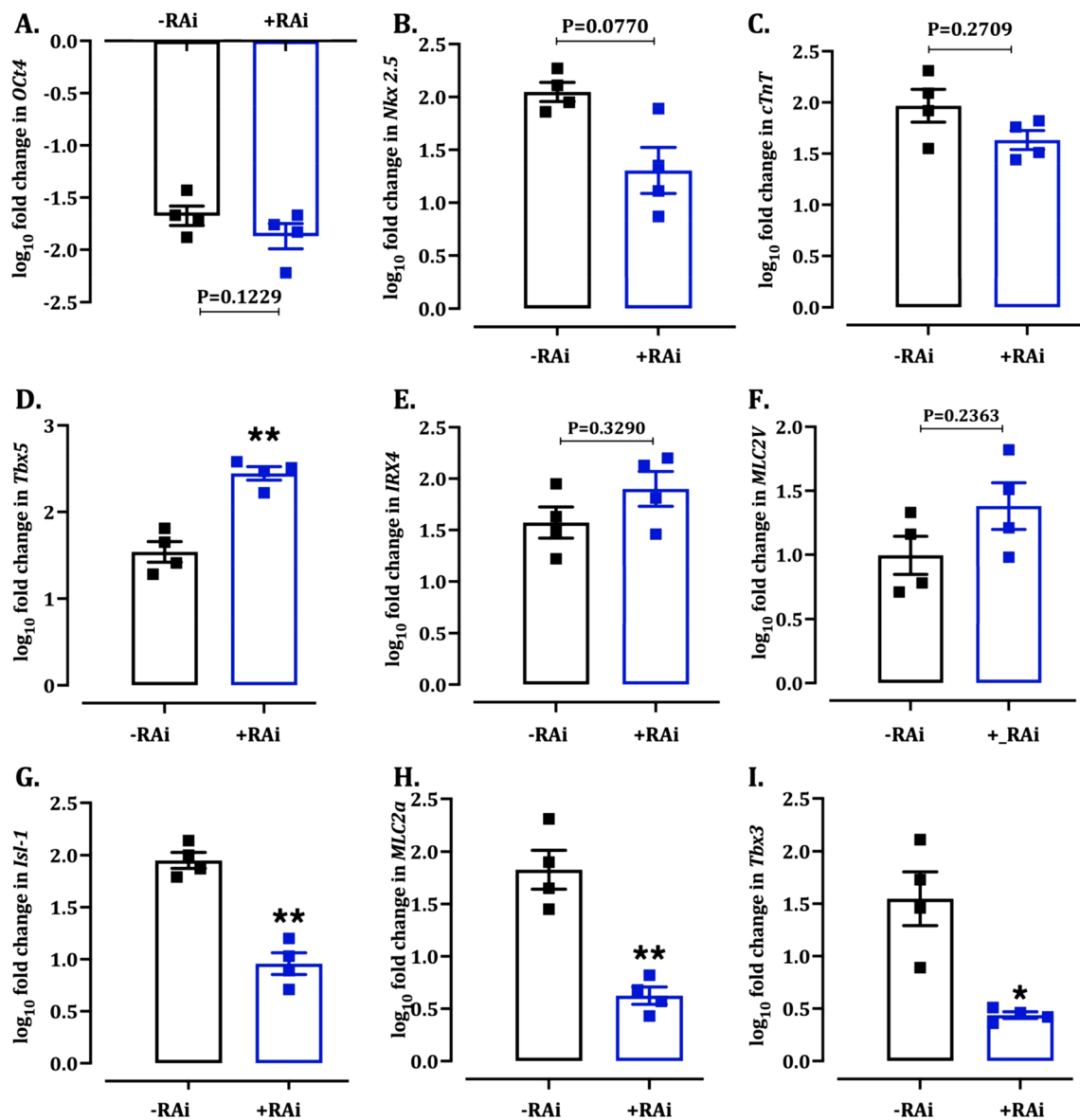


**Fig. 6** RT-PCR analysis of cardiac differentiation markers in mESCs differentiated by EB. Quantitative scatter plot bar graphs showing the expression of cardiac differentiation markers on day 14 of EB differentiation. The data were normalized to the gene expression of mESCs on day 0. Data were analysed by unpaired *t*-test and presented as mean ± SEM; \**P* < 0.05 and \*\**P* < 0.01 versus -RAi group. *n* = 4 independent repeats

ventricular chamber specification. In the current study, Nkx2.5 mRNA and protein levels were upregulated from day 5 of differentiation, implying the upregulation in the expression of a master regulator of various

ventricle-specific genes. While Nkx2.5 specifies a ventricular chamber identity, Tbx5 and Tbx3 are the transcription factors involved in the development of the left ventricle [28, 29] and pacemaker cells [30], respectively. Upregulation of

(See figure on next page.)

**Fig. 7** Ultrastructural features of mESCs differentiated by EB. **A–J**—representative transmission electron microscopy pictures of -RAi (**A–E**) and +RAi (**E–H**) cells. Yellow arrowhead—glycogen granules; pink arrowhead—collagen fibrils; N—nucleus; M—mitochondria; ER—endoplasmic reticulum. **K–N**—quantitative scatter plot bar graphs showing cell area (**K**), perimeter (**L**), circularity index (**M**) and mitochondrial number (**N**). Data were analysed by unpaired *t*-test with Welch’s correction and presented as mean ± SEM. \*\**P* < 0.01 and \*\*\*\**P* < 0.0001 versus -RAi group. *n* = 10 cells in each group

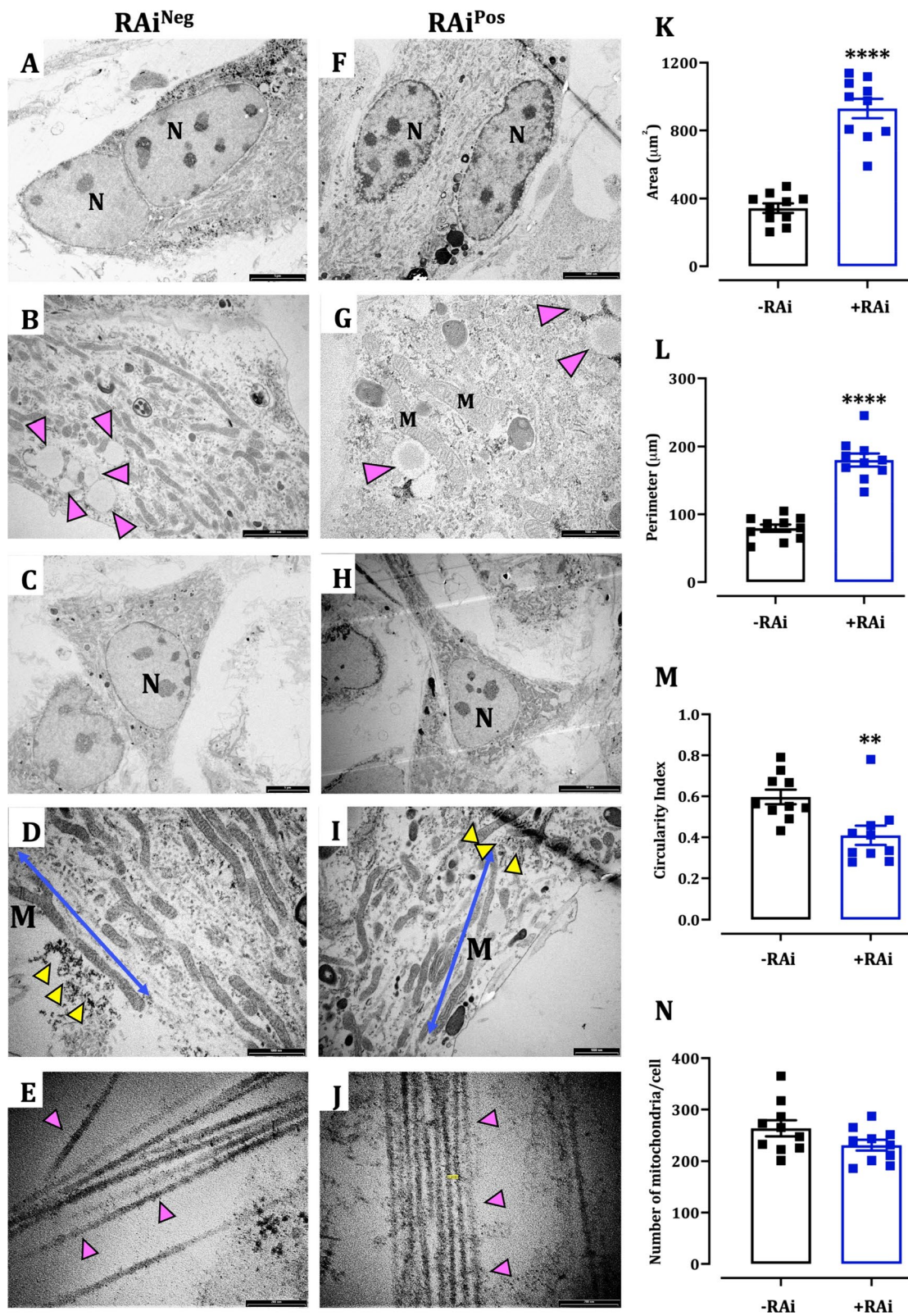


**Fig. 7** (See legend on previous page.)

both *Tbx5* and *Tbx3* from day 3 differentiation suggested an additional role of AA in specifying the ventricular and pacemaker progenitor pool. While *TBX5* gradually upregulated and sustained with RA inhibition, *Tbx3* showed a gradual downregulation suggesting that the current treatment protocol does not promote specification or differentiation into pacemaker cells. This could partially explain the absence of automaticity in our differentiated cells. Indeed, EBs differentiated in the absence of RAi exhibited spontaneous contraction.

Further, RA inhibition also induced downregulation of pro-atrial gene *MLC2a* while upregulating pro-ventricular gene *MLC2V*. Although we did not explore the underlying mechanism by which RAi causes ventricular lineage differentiation, Wang et al. demonstrated that the formation of an inhibitory complex by *IRX4* with retinoic X receptor (RXR) downregulated the expression of atrial-specific a unique myosin heavy chain (*AHMC1*), while promoting differentiation into the ventricular phenotype [31]. Based on this, upregulation of *IRX4* in our study following RAi possibly increased its binding to RXR, inducing ventricular lineage differentiation. This is further supported by reduced *IRX4* and *MLC2V* in EB-differentiated cells in which RA was not inhibited.

Monolayer differentiation resulted in cells displaying the features of immature embryonic cardiomyocytes such as deposition of glycogen granules, lipid droplets, and rough ER. Cardiac glycogen is present at high levels during early to mid-gestation before falling to low levels at the time of birth, thereby playing a critical role as an energy source during cardiogenesis [32]. Lipid droplets act as a triglyceride pool for the mitochondria that may serve as a crucial source of signalling intermediates to govern the mitochondrial function and fatty acid oxidation by regulating the expression of peroxisome proliferator-activated receptor-gamma coactivator-1-alpha (PGC-1 $\alpha$ ) and PGC-1-beta( $\beta$ ) and the activity of Peroxisome proliferator-activated receptor- $\alpha$  (PPAR- $\alpha$ ) [33]. Further, despite the expression of cTnT and  $\alpha$ -sarcomeric actin, the ultrastructural analysis failed to identify sarcomeres. Asmuda et al. demonstrated the expression of cTnT in the nucleus of neonatal cardiomyocytes, indicating that cardiac troponin and tropomyosin could have an important cellular function(s) beyond  $Ca^{2+}$  regulation [34]. Although monolayer differentiated cardiomyocytes expressed RyR2 (Additional file 1: Figure S5C), a protein channel responsible for balancing  $Ca^{2+}$  homeostasis by effluxing excess of  $Ca^{2+}$  from its  $Ca^{2+}$  store sarcoplasmic reticulum (SR) upon stimulation [35], they failed to emit any  $Ca^{2+}$  peaks when stimulated with  $Ca^{2+}$  infusion. This could be possibly due to the RyR2 channels being not sensitive enough to respond to their external calcium cues. Interestingly, differentiation by EB formation showed

mature cardiomyocyte phenotype, suggesting that mimicking embryonic morphogenesis results in the generation of morphologically and functionally mature CMs [36]. However, in spite of the expression of  $\alpha$ -sarcomeric actin, these cells still lack sarcomeres, which is a functional unit of the mature cardiomyocytes. Therefore, future studies should aim to focus on molecular pathways that could trigger the formation of sarcomeres required for functional excitation–contraction coupling.

## Conclusions

The current study features a novel protocol to differentiate mESCs into cardiomyocytes of ventricular lineage. Our results indicate that stage-specific combinatorial treatment with AA and Wnt and RA inhibition can induce differentiation of mESCs to ventricular lineage-specific cardiomyocytes by suppressing the expression of pro-atrial and pro-sinoatrial lineage. Differentiation via monolayer generated non-contracting ventricular-specific cardiomyocytes. EB generated cardiomyocytes were spontaneously contracting, which was not observed when treated with RA inhibitor, thereby demonstrating the importance of RA inhibition in shifting differentiation of cardiomyocytes towards ventricular lineage. Moreover, the electrically stimulated +RAi cells showed spontaneous contraction and  $Ca^{2+}$  release similar to –RAiEBs. Next critical step is to determine if in vivo transplantation of the homogenous population of cardiomyocytes that specifically express ventricular lineage markers into the ischemic left ventricle shows superior fusion with the host cardiomyocytes and exhibit better therapeutic efficacy. This will allow for a significant advancement in increasing the efficacy of stem cells therapy in regenerating the diseased heart. Moreover, with the recent use of induced pluripotent stem cells (iPSCs) in regenerative therapy in the clinic and its ability to differentiate into cardiomyocytes, it will be crucial to test the efficacy of our differentiation strategy in iPSCs to determine its translation ability [37].

## Abbreviations

AA: Ascorbic acid; AHMC1: Atrial-specific a unique myosin heavy chain; AM: Acetoxymethyl ester; cTnT: Cardiac troponin-T; Cx43: Connexin-43; DMEM: Dulbecco's modified eagle's medium; EB: Embryonic bodies; GFP: Green fluorescence protein; HAND2: Heart and neural crest derivatives expressed 2; HD: Hanging drop; IRX4: Iroquois homeobox 4; Isl-1: Islet-1; KDR: Kinase insert domain receptor; KRH buffer: Krebs-Ringer HEPES buffer; Mef2C: Myocyte enhancer factor 2C; Mesp-1: Mesoderm posterior protein 1; MLC-2a: Myosin regulatory light chain 2 atrial isoform; MLC-2V: Myosin regulatory light chain 2 ventricular isoform; PBS: Phosphate buffered saline; PGC-1 $\alpha$ : Peroxisome proliferator-activated receptor-gamma coactivator-1-alpha; PGC-1 $\beta$ : Peroxisome proliferator-activated receptor-gamma coactivator-1-beta; PPAR- $\alpha$ : Peroxisome proliferator-activated receptor- $\alpha$ ; RA: Retinoic acid; Rai: RA inhibitor; RXR: Retinoic X receptor; RYR2: Ryanodine receptor;  $\alpha$ -SA:  $\alpha$ -Sarcomeric actin; SR: Sarcoplasmic reticulum; T-Bry: T brachyury; *Tbx3*: T-box transcription factor 3; *Tbx5*: T-box transcription factor 5; TNG-A: A clone of transgenic Nanog.

## Supplementary Information

The online version contains supplementary material available at <https://doi.org/10.1186/s13287-022-02845-9>.

**Additional file 1. Figure S1. A.** Representative bright-field image of TNG-A mESCs aggregated in spherical colonies. **B.** A colony of TNG-A mESCs showing the endogenous expression of pluripotent nanog protein due to the *GFP* transgene tagged to *nanog*. Scale bar=100µm. **Figure S2. A&C.** Representative immunofluorescence images of mESCs on day 0 (**A**) and day 14 (time control, **C**) showing the expression of pluripotent markers (Oct4 and Sox2). Specificity of the antibody was confirmed by staining a independent samples with secondary controls only. **B&D.** Quantitative scatter plot bar graphs of RT-PCR analysis showing the expression of pluripotent markers gene *Nanog*, *Oct-4* and *Sox-2* in of mESCs on day 0 (**B**) and day 14 (time control, **G**). Mature mouse cardiomyocyte cell line HL-1 cells were used as negative controls. **Figure S3.** Representative confocal microscopy images showing the cells at different days of differentiation that are stained with secondary antibodies with the same labelling procedure without the primary antibody treatment, to rule out the non-specific binding of the secondary antibody. **Figure S4.** Quantitative scatter plot bar graphs of RT-PCR analysis showing the expression of cardiac differentiation genes in mESCs grown in differentiation medium with treatments (differentiated) and mESCs grown without any treatment (time control). Data were analyzed by unpaired t-test presented as Mean ± SEM. \*P<0.05, n=4 independent repeats. **Figure S5. A.** Representative image of Ca<sup>2+</sup> activity in a single differentiated mESC-CM on day 14 (**A**). The cells did not show any propensity to spontaneously release the calcium when induced with different concentrations of Ca<sup>2+</sup>. **B.** Quantitative scatter plot bar graphs showing a significant response of differentiated cells to caffeine-induced Ca<sup>2+</sup> release **C.** Quantitative scatter plot bar graphs of RT-PCR analysis showing the expression of *RYR2* after 14 days of differentiation. Data were analyzed by unpaired t-test with Welch's correction. \*\*\*P<0.01 and \*\*\*\*P<0.0001 vs. differentiated cells. Data presented as Mean ± SEM. n=35 cells from three independent experiments in **B** n=4 independent experiments in **C**. **Figure S6.** Representative bright field microscopic images of m-ESC over 14days of cultivation by EB method. On day 2 (**A**) the EBs were generated and transferred to a petri dish. The colony was preserved and the EB was still in three-dimensional shape on day 3 (**B**). On day 4 (**C**) the EBs were transferred to gelatin coated plates and finally on day 5(**D**) the EB adhering to the plate was observed. From day 6 (**E**) the images were taken at a magnification of 40x to observe closer morphological changes. Cells looked more spherical and the cells were observed very close together. Over the period of day 7(**F**), 8 (**G**), 9(**H**), 10(**I**), 11(**J**), 12(**K**), 13(**L**), 14(**M**), the morphology of cells became more elongated and also the myotube formation was observed. Clear morphological differences can be seen comparing undifferentiated ESC (**N**) and differentiated cardiomyocytes on day14 (**O**). Scale bars are 500 µM for A-D, 200 µM for E-M and 00 µM for N&O. **Figure S7. A–B.** Representative confocal microscopy images showing the expression of cardiac transcription factors Nkx2.5 (**A**) and Isl-1 (**B**) in differentiated and undifferentiated mESCs by EB method. **C.** Representative confocal microscopy images showing the expression of ventricular cardiomyocytes markers IRX4 and MLC2V following differentiation of mESCs by EB method in both +RAi and -RAi groups. **D–E.** Representative confocal microscopy images showing the expression of ventricular cardiomyocytes markers Mef2c (**D**) and Cx43(**E**) in differentiated and undifferentiated mESCs by EB method. **F.** Representative flowcytometry gating images showing the expression of left ventricular cardiomyocytes marker IRX4 and cTnt following differentiation of mESCs by EB method in both +RAi and -RAi groups. **Figure S8.** Uncropped western blots of Connexin43 (Cx43) and GAPDH represented in Figure 3C (**A**) and MLC2V and GAPDH represented in Figure 3D (**B**).

## Acknowledgements

We thank Mr. Richard Easingwood of transmission electron microscopy facility, Mr. Andrew McNaughton of confocal facility and Ms. Katie Young of Flow cytometry facility for their technical help.

## Author contributions

R.S. conducted the study, analysed the data and wrote the first draft of the manuscript. S.L. and R.S. established the technique of EB formation. J.B.P. performed additional experiments requested by the reviewers. T.H. provided access to the mouse embryonic stem cells and made critical review of the manuscript. A.C. helped in conducted calcium signalling experiments. P.J. supervised and guided in analysis of calcium signalling experiments and made critical review of the manuscript. R.R.L. co-designed the study and made critical review of the manuscript. R.K. designed the study, overviewed the project, helped in data analysis, wrote the funding application and finalized the manuscript. All authors read and approved the final manuscript.

## Funding

This study was supported by a small project funding from Heart Foundation (1698) and the Department of Physiology Ph.D. consumables fund. Mr Satthenapalli was supported by the University of Otago Doctoral Scholarship.

## Availability of data and materials

All the data are included in the manuscript.

## Declarations

### Ethics approval and consent to participate

Not applicable.

### Consent for publication

Not applicable.

### Competing interests

The authors declare that they have no competing interests.

## Author details

<sup>1</sup>Department of Physiology, HeartOtago, School of Biomedical Sciences, University of Otago, 270, Great King Street, Dunedin 9010, New Zealand. <sup>2</sup>Department of Anatomy, School of Biomedical Sciences, University of Otago, Dunedin 9010, New Zealand. <sup>3</sup>Oklahoma Medical Research Foundation, Oklahoma City, USA.

Received: 26 October 2021 Accepted: 11 April 2022

Published online: 06 May 2022

## References

- Isomi M, Sadahiro T, Ieda M. Progress and challenge of cardiac regeneration to treat heart failure. *J Cardiol*. 2019;73(2):97–101.
- Satthenapalli VR, Lamberts RR, Katare RG. Concise review: challenges in regenerating the diabetic heart: a comprehensive review. *Stem Cells*. 2017;35(9):2009–26.
- Tzahor E, Poss KD. Cardiac regeneration strategies: staying young at heart. *Science*. 2017;356(6342):1035–9.
- Matsa E, Burrige PW, Wu JC. Human stem cells for modeling heart disease and for drug discovery. *Sci Transl Med*. 2014;6(239):239ps6.
- Wang WE, Chen X, Houser SR, Zeng C. Potential of cardiac stem/progenitor cells and induced pluripotent stem cells for cardiac repair in ischaemic heart disease. *Clin Sci (Lond)*. 2013;125(7):319–27.
- Bussey CT, Hughes G, Saxena P, Galvin IF, Bunton RW, Noye MK, et al. Chamber-specific changes in calcium-handling proteins in the type 2 diabetic human heart with preserved ejection fraction. *Int J Cardiol*. 2015;193:53–5.
- He JQ, Ma Y, Lee Y, Thomson JA, Kamp TJ. Human embryonic stem cells develop into multiple types of cardiac myocytes: action potential characterization. *Circ Res*. 2003;93(1):32–9.
- Moore JC, Fu J, Chan YC, Lin D, Tran H, Tse HF, et al. Distinct cardiogenic preferences of two human embryonic stem cell (hESC) lines are imprinted in their proteomes in the pluripotent state. *Biochem Biophys Res Commun*. 2008;372(4):553–8.
- Epstein JA, Franklin H. Epstein lecture. Cardiac development and implications for heart disease. *N Engl J Med*. 2010;363(17):1638–47.

10. Ng SY, Wong CK, Tsang SY. Differential gene expressions in atrial and ventricular myocytes: insights into the road of applying embryonic stem cell-derived cardiomyocytes for future therapies. *Am J Physiol Cell Physiol*. 2010;299(6):C1234–49.
11. Cecchetto A, Rampazzo A, Angelini A, Bianco LD, Padalino M, Stellin G, et al. From molecular mechanisms of cardiac development to genetic substrate of congenital heart diseases. *Future Cardiol*. 2010;6(3):373–93.
12. Roche P, Czubryt M, Wigle J. Molecular mechanisms of cardiac development. In: Ostadal B, Dhalla NS, editors. *Cardiac adaptations*. New York: Springer; 2013. p. 19–39.
13. Lian X, Hsiao C, Wilson G, Zhu K, Hazeltine LB, Azarin SM, et al. Robust cardiomyocyte differentiation from human pluripotent stem cells via temporal modulation of canonical Wnt signaling. *Proc Natl Acad Sci U S A*. 2012;109(27):E1848–57.
14. Takahashi T, Lord B, Schulze PC, Fryer RM, Sarang SS, Gullans SR, et al. Ascorbic acid enhances differentiation of embryonic stem cells into cardiac myocytes. *Circulation*. 2003;107(14):1912–6.
15. Cao N, Liu Z, Chen Z, Wang J, Chen T, Zhao X, et al. Ascorbic acid enhances the cardiac differentiation of induced pluripotent stem cells through promoting the proliferation of cardiac progenitor cells. *Cell Res*. 2012;22(1):219–36.
16. Gassanov N, Er F, Zagidullin N, Jankowski M, Gutkowska J, Hoppe UC. Retinoid acid-induced effects on atrial and pacemaker cell differentiation and expression of cardiac ion channels. *Differentiation*. 2008;76(9):971–80.
17. Ficiz G, Hore TA, Santos F, Lee HJ, Dean W, Arand J, et al. FGF signaling inhibition in ESCs drives rapid genome-wide demethylation to the epigenetic ground state of pluripotency. *Cell Stem Cell*. 2013;13(3):351–9.
18. Chambers I, Silva J, Colby D, Nichols J, Nijmeijer B, Robertson M, et al. Nanog safeguards pluripotency and mediates germline development. *Nature*. 2007;450(7173):1230–4.
19. Dixit P, Donnelly H, Edamatsu M, Galvin I, Bunton R, Katare R. Progenitor cells from atria, ventricle and peripheral blood of the same patients exhibit functional differences associated with cardiac repair. *Int J Cardiol*. 2017;228:412–21.
20. Bondue A, Lapouge G, Paulissen C, Semeraro C, Iacovino M, Kyba M, et al. Mesp1 acts as a master regulator of multipotent cardiovascular progenitor specification. *Cell Stem Cell*. 2008;3(1):69–84.
21. Gao X-F, Zhou Y, Wang D-Y, Lew K-S, Richards AM, Wang P. Urocortin-2 suppression of p38-MAPK signaling as an additional mechanism for ischemic cardioprotection. *Mol Cell Biochem*. 2015;398(1):135–46.
22. Lian X, Zhang J, Azarin SM, Zhu K, Hazeltine LB, Bao X, et al. Directed cardiomyocyte differentiation from human pluripotent stem cells by modulating Wnt/ $\beta$ -catenin signaling under fully defined conditions. *Nat Protoc*. 2013;8(1):162–75.
23. Zhang Q, Jiang J, Han P, Yuan Q, Zhang J, Zhang X, et al. Direct differentiation of atrial and ventricular myocytes from human embryonic stem cells by alternating retinoid signals. *Cell Res*. 2011;21(4):579–87.
24. Abbey D, Seshagiri PB. Ascorbic acid-mediated enhanced cardiomyocyte differentiation of mouse ES-cells involves interplay of DNA methylation and multiple-signals. *Differentiation*. 2017;96:1–14.
25. Dodou E, Verzi MP, Anderson JR, Xu SM, Black BL. Mef2c is a direct transcriptional target of ISL1 and GATA factors in the anterior heart field during mouse embryonic development. *Development*. 2004;131(16):3931–42.
26. Bruneau BG, Bao ZZ, Tanaka M, Schott JJ, Izumo S, Cepko CL, et al. Cardiac expression of the ventricle-specific homeobox gene *Irx4* is modulated by *Nkx2-5* and *dHand*. *Dev Biol*. 2000;217(2):266–77.
27. Targoff KL, Colombo S, George V, Schell T, Kim SH, Solnica-Krezel L, et al. *Nkx* genes are essential for maintenance of ventricular identity. *Development*. 2013;140(20):4203–13.
28. Takeuchi JK, Ohgi M, Koshiba-Takeuchi K, Shiratori H, Sakaki I, Ogura K, et al. *Tbx5* specifies the left/right ventricles and ventricular septum position during cardiogenesis. *Development*. 2003;130(24):5953–64.
29. Plegeman TF Jr, Yutzey KE. Differential expression and function of *Tbx5* and *Tbx20* in cardiac development. *J Biol Chem*. 2004;279(18):19026–34.
30. Hoogaars WM, Engel A, Brons JF, Verkerk AO, de Lange FJ, Wong LY, et al. *Tbx3* controls the sinoatrial node gene program and imposes pacemaker function on the atria. *Genes Dev*. 2007;21(9):1098–112.
31. Wang GF, Nikovits W, Bao Z-Z, Stockdale FE. *Irx4* forms an inhibitory complex with the vitamin D and retinoic X receptors to regulate cardiac chamber-specific slow MyHC3Expression. *J Biol Chem*. 2001;276(31):28835–41.
32. Dawes GS, Mott JC, Shelley HJ. The importance of cardiac glycogen for the maintenance of life in foetal lambs and newborn animals during anoxia. *J Physiol*. 1959;146(3):516–38.
33. Haemmerle G, Moustafa T, Woelkart G, Buttner S, Schmidt A, van de Weijer T, et al. ATGL-mediated fat catabolism regulates cardiac mitochondrial function via PPAR-alpha and PGC-1. *Nat Med*. 2011;17(9):1076–85.
34. Asumda FZ, Chase PB. Nuclear cardiac troponin and tropomyosin are expressed early in cardiac differentiation of rat mesenchymal stem cells. *Differentiation*. 2012;83(3):106–15.
35. Munro ML, Jones PP. Too much of a good thing? Establishing a role of excessive RyR2 dephosphorylation in heart disease. *J Physiol*. 2020;598(6):1115–6.
36. Boheler KR, Czyz J, Tweedie D, Yang HT, Anisimov SV, Wobus AM. Differentiation of pluripotent embryonic stem cells into cardiomyocytes. *Circ Res*. 2002;91(3):189–201.
37. Deinsberger J, Reisinger D, Weber B. Global trends in clinical trials involving pluripotent stem cells: a systematic multi-database analysis. *NPJ Regen Med*. 2020;5:15.

## Publisher's Note

Springer Nature remains neutral with regard to jurisdictional claims in published maps and institutional affiliations.

Ready to submit your research? Choose BMC and benefit from:

- fast, convenient online submission
- thorough peer review by experienced researchers in your field
- rapid publication on acceptance
- support for research data, including large and complex data types
- gold Open Access which fosters wider collaboration and increased citations
- maximum visibility for your research: over 100M website views per year

At BMC, research is always in progress.

Learn more [biomedcentral.com/submissions](https://biomedcentral.com/submissions)

